JACS
JOURNAL OF THE AMERICAN CHEMICAL SOCIETY
Article
pubs.acs.org/JACS

Use of ^{77}Se and ^{125}Te NMR Spectroscopy to Probe Covalency of the Actinide-Chalcogen Bonding in $[Th(E_n)\{N(SiMe_3)_2\}_3]^-$ (E = Se, Te; n = 1, 2) and Their Oxo-Uranium(VI) Congeners

Danil E. Smiles,[†] Guang Wu,[†] Peter Hrobárik,*[,‡] and Trevor W. Hayton*[,†]

[†]Department of Chemistry and Biochemistry, University of California, Santa Barbara, California 93106, United States
[‡]Institut für Chemie, Technische Universität Berlin, Strasse des 17. Juni 135, 10623 Berlin, Germany

Supporting Information

ABSTRACT: Reaction of $[Th(I)(NR_2)_3]$ (R = $SiMe_3$) (**1**) with 1 equiv of either $[K(18\text{-crown-}6)]_2[Se_4]$ or $[K(18\text{-crown-}6)]_2[Te_2]$ affords the thorium dichalcogenides, $[K(18\text{-crown-}6)][Th(\eta^2\text{-}E_2)(NR_2)_3]$ (E = Se, **2**; E = Te, **3**), respectively. Removal of one chalcogen atom via reaction with Et_3P, or Et_3P and Hg, affords the monoselenide and monotelluride complexes of thorium, $[K(18\text{-crown-}6)][Th(E)(NR_2)_3]$ (E = Se, **4**; E = Te, **5**), respectively. Both **4** and **5** were characterized by X-ray crystallography and were found to feature the shortest known Th−Se and Th−Te bond distances. The electronic structure and nature of the actinide-chalcogen bonds were investigated with ^{77}Se and ^{125}Te NMR spectroscopy accompanied by detailed quantum-chemical analysis. We also recorded the ^{77}Se NMR shift for a U(VI) oxo-selenido complex, $[U(O)(Se)(NR_2)_3]^-$ ($\delta(^{77}Se)$ = 4905 ppm), which features the highest frequency ^{77}Se NMR shift yet reported, and expands the known ^{77}Se chemical shift range for diamagnetic substances from ∼3300 ppm to almost 6000 ppm. Both ^{77}Se and ^{125}Te NMR chemical shifts of given chalcogenide ligands were identified as quantitative measures of the An−E bond covalency within an isoelectronic series and supported significant 5f-orbital participation in actinide−ligand bonding for uranium(VI) complexes in contrast to those involving thorium(IV). Moreover, X-ray diffraction studies together with NMR spectroscopic data and density functional theory (DFT) calculations provide convincing evidence for the actinide−chalcogen multiple bonding in the title complexes. Larger An−E covalency is observed in the $[U(O)(E)(NR_2)_3]^-$ series, which decreases as the chalcogen atom becomes heavier.

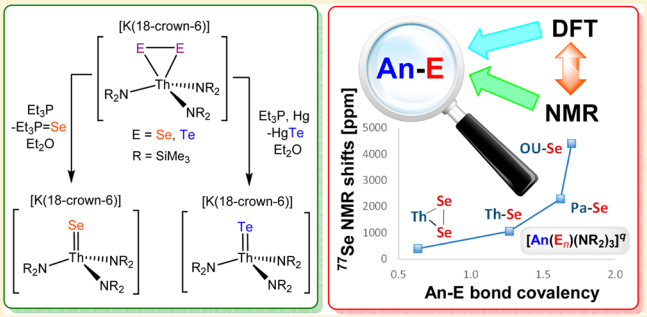

INTRODUCTION

The recent interest in covalency and f orbital participation in An-L bonding[1] has sparked increased attention toward the synthesis and study of actinide-ligand multiple bonds. These functional groups have proven to be a promising avenue for the better understanding of bonding interactions in actinide systems;[1b−d,2] however, the vast majority of this work has been performed with uranium.[3,4] In contrast, complexes with metal−ligand multiple bonds of the other actinides, such as thorium, are much less common. For example, a few thorium imido complexes have been reported, which mostly feature the metallocene architecture.[5] In addition, two thorium oxo complexes are known,[5a,6] while only one thorium sulfide has been characterized so far, namely, $[K(18\text{-crown-}6)][Th(S)(NR_2)_3]$ (R = $SiMe_3$).[6] Surprisingly, no molecular thorium selenide or telluride complexes are known, making them an obvious target for synthesis. In fact, even thorium selenate complexes are rare,[5b,c,7] while there are no structurally characterized coordination complexes containing Th−Te bonds.[8] In addition to addressing their rarity, the synthesis of thorium selenides and tellurides would be of interest for another reason, namely, the ability to use ^{77}Se and ^{125}Te NMR spectroscopies to probe the extent of covalency in actinide-ligand bonding. Previously, we demonstrated that ^{13}C and ^{1}H NMR shifts could be used to estimate 5f orbital participation in Th(IV) and U(VI) alkyls and hydrides via spin−orbit-induced deshielding.[9,10] The synthesis and characterization of monoselenides and tellurides would allow us to extend this analysis to An−E multiple bonds for the first time. Although analogous NMR probes exist for the oxo (^{17}O) and sulfido (^{33}S) ligated complexes, there is a lack of such studies due to difficulties associated with their very low natural abundance and the quadrupolar moments of these nuclei, which cause considerable broadening of the NMR peaks.[11] Surprisingly, there are also only a few NMR studies of molecular transition-metal selenides and tellurides.

Herein, we report the synthesis and structural and NMR spectral characterization of the mono- and dichalcogenide complexes $[K(18\text{-crown-}6)][Th(E_n)(NR_2)_3]$ (E = Se, Te; n =

Received: July 24, 2015
Published: December 14, 2015

DOI: 10.1021/jacs.5b07767
J. Am. Chem. Soc. 2016, 138, 814−825

1, 2), along with an investigation into their electronic structures. To understand the nature of actinide-chalcogen bonds in these complexes in more detail, DFT analysis of the recorded ^{77}Se and ^{125}Te NMR chemical shifts and of the An−E bonding were performed and the results are contrasted with those of the closed-shell oxo-uranium(VI) complexes $[U(O)(E)(NR_2)_3]^-$.

RESULTS AND DISCUSSION

Synthesis. We recently reported the use of the polychalcogenides $[E_n]^{2-}$ (E = Se, n = 4; E = Te, n = 2) to access the uranium(IV) chalcogenide complexes, $[K(18\text{-crown-6})][U(\eta^2\text{-}E_2)(NR_2)_3]$ (E = Se, Te), via salt metathesis with $[U(I)(NR_2)_3]$.[4h] Similarly, the thorium iodide, $[Th(I)(NR_2)_3]$ (**1**),[6] has proven to be a viable entry point to the synthesis of the analogous thorium dichalcogenides. Thus, addition of 1 equiv of $[K(18\text{-crown-6})]_2[Se_4]$, to a suspension of **1** in THF affords an orange solution, concomitant with the formation of a black precipitate. From the resulting mixture we isolated the thorium diselenide, $[K(18\text{-crown-6})]_2[Th(\eta^2\text{-}Se_2)(NR_2)_3]$ (**2**), in 63% yield after crystallization from Et_2O (Scheme 1). Notably, only

Scheme 1. Syntheses of Complexes 2 and 3

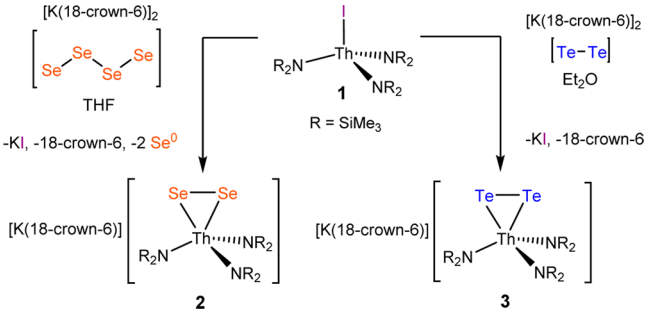

two Se atoms from the starting tetraselenide are incorporated into **2**. Presumably, the coordination of more than two Se atoms to Th is too sterically demanding and the extra Se atoms in $[Se_4]^{2-}$ are ejected as Se^0. This hypothesis is supported by the black precipitate that is formed during the course of the reaction. Similarly, reaction of 1 equiv of $[K(18\text{-crown-6})]_2[Te_2]$ with **1** in Et_2O affords a dark green solution. Crystallization from Et_2O affords the thorium ditelluride, $[K(18\text{-crown-6})][Th(\eta^2\text{-}Te_2)(NR_2)_3]$ (**3**), as a green crystalline solid in 36% yield.

Complexes **2** and **3** have both proven to be competent precursors to the corresponding monochalcogenides. Thus, the addition of 1 equiv of Et_3P to an orange solution of **2** in Et_2O results in a gradual bleaching of the color. From this colorless solution we isolated the thorium monoselenide, $[K(18\text{-crown-6})][Th(Se)(NR_2)_3]$ (**4**), as colorless crystalline solid in 53% yield after workup (Scheme 2). This synthetic strategy has been deployed several times in the past.[4h,12] In addition to complex **4**, we also observe the formation of $Et_3P{=}Se$, which can be isolated as an off-white solid in 97% yield. The identity of this species was confirmed by comparison of its $^{31}P\{^1H\}$ and $^{77}Se\{^1H\}$ NMR spectra to that of authentic material (Figure S13 and S14).[13] We then endeavored to apply a similar strategy toward the synthesis of a monotelluride complex from complex **3**. However, addition of 1 equiv of Et_3P to a solution of **3**, in benzene-d_6, results in no reaction after 24 h, as determined by ^1H and $^{31}P\{^1H\}$ NMR spectroscopies (Figures S27−S28). We

Scheme 2. Syntheses of Complexes 4 and 5

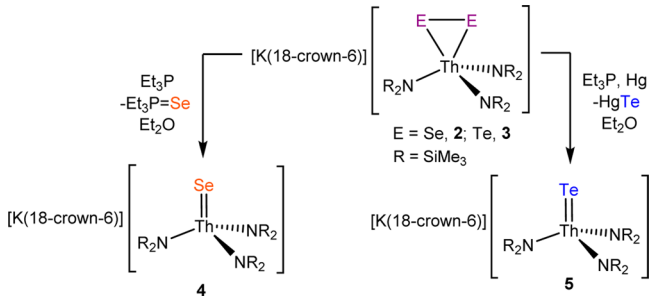

then sought an alternate route for the synthesis of the monotelluride complex. Previously, Parkin and co-workers reported the conversion of the ditelluride complex, $[Cp^*_2Ta(\eta^2\text{-}Te_2)(H)]$, into the corresponding monotelluride, $[Cp^*_2Ta(Te)(H)]$, via reaction with Et_3P and Hg.[14] In this example, the addition of Hg to the reaction mixture is likely needed to provide the required thermodynamic driving force for Te abstraction (as formation of a P═Te bond is probably not sufficient), while Et_3P functions as a Te-transfer catalyst.[15] Gratifyingly, addition of excess Hg and excess Et_3P to a green solution of **3**, in Et_2O, affords a colorless solution and a dark black precipitate (presumably HgTe) after 24 h. Filtration and removal of the volatiles in vacuo affords the first thorium monotelluride, $[K(18\text{-crown-6})][Th(Te)(NR_2)_3]$ (**5**), as a colorless powder in 78% yield (Scheme 2).

X-ray Crystallography. Complexes **2** and **3** both crystallize in the triclinic space group $P\bar{1}$ as diethyl ether solvates, **2**·0.5Et_2O and **3**·0.5Et_2O, and their solid-state molecular structures are shown in Figure 1 (see also Table 1 for comparison of the selected structural parameters with those optimized at the DFT level for the complete dichalcogenide family, $[K(18\text{-crown-6})][Th(\eta^2\text{-}E_2)(NR_2)_3]$). Complexes **2** and **3** are isostructural to their uranium(IV) analogues, and feature distorted pseudotetrahedral geometries about the thorium centers (**2**: N1−Th1−N2 = 99.8(2)°, N2−Th1−N3 = 110.1(2), N1−Th1−N3 = 125.4(2)°; **3**: N1−Th1−N2 = 126.8(1), N2−Th1−N3 = 108.9(1), N1−Th1−Th3 = 100.8(1)°). This distortion is a result of the steric crowding between the $[\eta^2\text{-}E_2]^{2-}$ moiety and the large $[N(SiMe_3)_2]^-$ ligands. The Th−Se distances in **2** (Th−Se = 2.8750(7) and 2.9555(7) Å) are comparable to previously reported Th−Se single bonds.[5b,c,7b] For example, the average Th−Se bond length in $[Th(Se_2P(C_6H_5)(OMe))_4]$ is 3.027 Å,[5c] while the average Th−Se bond length in $[(\eta^5\text{-}1,3\text{-}(Me_3C)_2C_5H_3)_2Th(SePh)_2]$ is 2.88 Å.[5b] For further comparison, the average Th−Se distance in $ThSe_2$ is 3.06 Å (with d(Th−Se) ranging from 2.85 to 3.27 Å).[16] The Th−Te distances of **3** (Th1−Te1 = 3.1076(4) and Th1−Te2 = 3.2375(4) Å) are longer than the Th−Se bond distances of **2**, consistent with the larger ionic radii of Te^{2-} versus Se^{2-}.[17] While no other coordination complexes with Th−Te bonds have been reported,[8] several solid-state thorium tellurides are known, including KTh_2Te_6,[18] $ThTe_2I_2$,[19] and Th_7Te_{12}.[20] These materials feature comparable Th−Te distances, ranging from 3.137(2) to 3.483(1) Å.[18−20] The Se−Se bond distance in **2** (2.397(1) Å) is comparable to those of the analogous uranium complex, $[K(18\text{-crown-6})][U(\eta^2\text{-}Se_2)(NR_2)_3]$ (av. Se−Se = 2.367 Å),[4h] consistent with the structural similarities between these species. Likewise, the Te−Te bond distance in **3** (2.7525(5) Å), is similar to that of its uranium analogue, $[K(18\text{-crown-6})][U(\eta^2\text{-}Te_2)(NR_2)_3]$

DOI: 10.1021/jacs.5b07767
J. Am. Chem. Soc. 2016, 138, 814−825

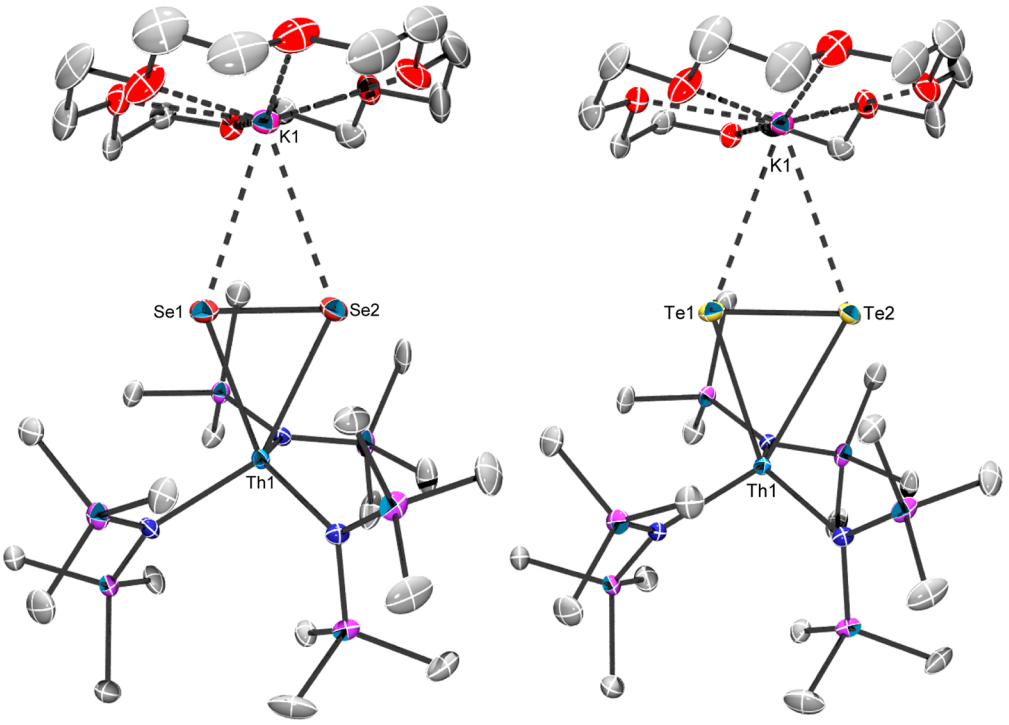

Figure 1. Solid state molecular structures of complexes **2**·0.5Et_2O (left) and **3**·0.5Et_2O (right), with 50% probability ellipsoids. Diethyl ether solvates and hydrogen atoms are omitted for clarity.

Table 1. Selected Bond Distances (Å) for [K(18-crown-6)][Th(η^2-E_2)(NR_2)$_3$] (E = O, S, Se, Te)

		chalcogen atom, E			
bond	method	O	S	Se (**2**)	Te (**3**)
Th−E (av.)	X-ray	–	–	2.915	3.173
	calcd.[a]	2.199	2.741	2.914	3.180
E−E	X-ray	–	–	2.397(1)	2.7525(5)
	calcd.[a]	1.472	2.102	2.379	2.749
E−K (av.)	X-ray	–	–	3.433	3.661
	calcd.[a]	2.667	3.149	3.304	3.512
Th−N (av.)	X-ray	–	–	2.354	2.345
	calcd.[a]	2.391	2.342	2.330	2.318

[a]Structure optimized at the PBE0-D3(BJ)/def2-TZVP/ECP level of theory (cf. Computational Details).

(Te1−Te2 = 2.7456(4) Å).[4h] The $[E_2]^{2-}$ ligands in **2** and **3** also exhibit dative interactions with the K^+ ion of the $[K(18\text{-crown-6})]^+$ moiety. The E−K distances in **2** (Se1−K1 = 3.425(2) and Se2−K1 = 3.441(2) Å) and **3** (Te1−K1 = 3.6534(9) and Te2−K1 = 3.6682(9) Å) are comparable to those of their uranium(IV) analogues as well as those of the corresponding polychalcogenide salts.

Complex **4** crystallizes in the triclinic space group $P\bar{1}$, with two molecules in the asymmetric unit, while complex **5** crystallizes in the triclinic spacegroup $P\bar{1}$ as a diethyl ether solvate **5**·0.5Et_2O, with four independent molecules in its asymmetric unit. Their solid-state molecular structures are shown in Figure 2, while selected bond lengths and angles are presented in Table 2. Complex **4** is structurally identical to the previously reported thorium monochalcogenides, [K(18-crown-6)][Th(E)(NR_2)$_3$] (E = O, S),[6] as well as its uranium(IV) analogue [K(18-crown-6)][U(Se)(NR_2)$_3$].[4h] In the solid-state, complex **4** features a pseudotetrahedral geometry (av. N−Th−N = 116.4° and av. N−Th−Se = 101.0°) about the thorium ion. The Th−Se distances in **4** (2.6497(7) and 2.6566(7) Å) are significantly shorter than those of complex **2**, indicating the multiple bond character of the Th−Se interaction (see below for DFT analysis). Finally, the Se−K distances in **4** (Se1−K1 = 3.125(2) and Se2−K2 = 3.201(2) Å) are slightly shorter than those in complex **2**, but are comparable to those of the isostructural uranium(IV) complex.

Complex **5** is isostructural to its tetravalent uranium analogue. In the solid-state, **5** features a pseudotetrahedral geometry about the Th center (av. N−Th−N = 112.9°), akin to that observed for complex **4**. The Th−Te distances in **5** (av. 2.933 Å) are the shortest Th−Te distances reported, and are significantly shorter than those of complex **3**,[18−21] suggestive of multiple bond character in this linkage. The E−K distances of **5** (av. 3.437 Å) are longer than the structurally identical oxo, sulfido, and selenido complexes (O−K = 2.645(7), av. S−K = 3.081, av. Se−K = 3.163), consistent with the increase in ionic radii of Te^{2-} versus O^{2-}, S^{2-} and Se^{2-}.[17a]

Spectroscopic Characterization. The ^{1}H NMR spectra of complexes **2** and **4**, in benzene-d_6, both feature two sharp resonances (**2**: 0.74 and 3.17 ppm; **4**: 0.76 and 3.17 ppm) in a 54:24 ratio, assignable to the methyl groups of the silylamide ligands and the methylene groups of the 18-crown-6 moiety, respectively. Not surprisingly, the ^{1}H NMR spectra of **3** and **5**, in benzene-d_6, are nearly identical to those of their selenide analogues. Each spectrum again features two sharp resonances (**3**: 0.79 and 3.14 ppm; **5**: 0.81 and 3.15 ppm) in a 54:24 ratio, assignable to the methyl groups of the silylamide ligands and the methylene groups of the 18-crown-6 moiety, respectively.

We also characterized complexes **2**−**5** by either ^{77}Se{^{1}H} or ^{125}Te{^{1}H} NMR spectroscopy. The ^{77}Se{^{1}H} NMR spectrum of **2**, in benzene-d_6, exhibits a single peak at 246 ppm, which is assignable to the $[\eta^2\text{-}Se_2]^{2-}$ ligand. This resonance is within the range previously reported for the $[\eta^2\text{-}Se_2]^{2-}$ ligand (−408−1252 ppm).[22] Notably, this signal shifts to 302 ppm in pyridine-

DOI: 10.1021/jacs.5b07767
J. Am. Chem. Soc. 2016, 138, 814−825

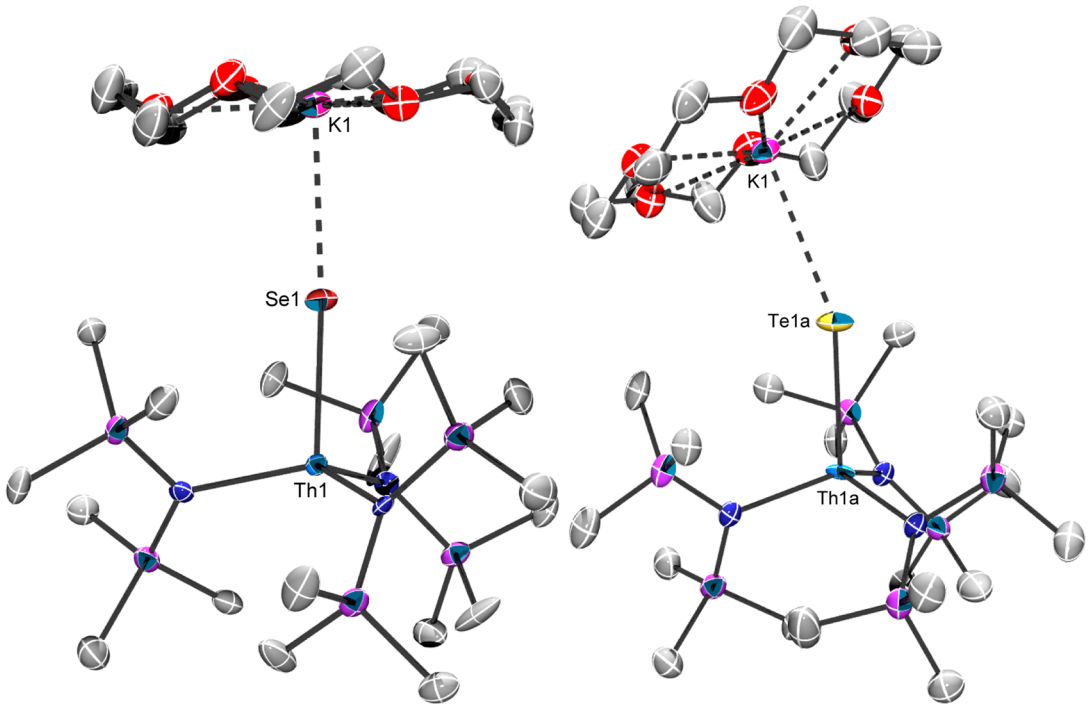

Figure 2. Solid state molecular structures of complex **4** (left), and complex **5**·0.5Et_2O (right) with 50% probability ellipsoids. Three molecules of **5**, diethyl ether solvates and hydrogen atoms are omitted for clarity.

Table 2. Selected Bond Distances (Å) and Angles (deg) for [K(18-crown-6)][Th(E)$(NR_2)_3$] (E = O, S, Se, Te)

		chalcogen atom, E			
bond	method	O	S	Se (**4**)	Te (**5**)
Th−E (av.)	X-ray	1.983(7)[a]	2.516[a]	2.653	2.933
	calcd.[b]	1.965	2.520	2.674	2.922
E−K (av.)	X-ray	2.645(7)[a]	3.081[a]	3.163	3.437
	calcd.[b]	2.626	2.991	3.154	3.323
Th−N (av.)	X-ray	2.42[a]	2.36[a]	2.35	2.37
	calcd.[b]	2.401	2.345	2.334	2.332
N−Th−N (av.)	X-ray	115.6	116.6	116.4	112.9
	calcd.[b]	115.9	117.1	117.0	115.9
Th−E−K (av.)	X-ray	167.5(4)[a]	163.6[a]	162.8	143.5[c]
	calcd.[b]	155.1	178.8	160.3	153.2

[a]Taken from ref 6. [b]Structure optimized at the PBE0-D3(BJ)/def2-TZVP/ECP level of theory (cf. Computational Details). [c]The Th−Te−K angles in **5** span a large range (122.8(8)° to 160.8(8)°).

d_5, which is reflective of the formation of separated cation/anion pair in this solvent (see below for further discussion). Complex **4** exhibits a single resonance, shifted downfield from that of **2**, at 885 ppm in benzene-d_6, assignable to the $[Se]^{2-}$ ligand. This resonance appears at 992 ppm in pyridine-d_5, whereby the deshielding in this solvent can be primarily attributed, again, to a disruption of the contact ion pair. Both values are within the reported range for terminal transition metal $[Se]^{2-}$ complexes (700−2400 ppm).[22e,23] For further comparison, Th$[Se_2P(C_6H_5)(OMe)]_4$ features a peak at 222 ppm in its ^{77}Se NMR spectrum. This example is the only other reported ^{77}Se chemical shift for a selenium bound to thorium.[5c] The ^{125}Te{^{1}H} NMR spectra of complexes **3** and **5** each feature a singlet at −351 and 481 ppm in benzene-d_6, assignable to the $[\eta^2\text{-}Te_2]^{2-}$ and $[Te]^{2-}$ moieties, respectively. In pyridine-d_5, resonances of **3** and **5** exhibit high-frequency (downfield) shifts to −272 and 628 ppm, respectively, which we attribute similarly to a disruption of the contact ion pair. Moreover, these resonances fall within the respective ranges of other complexes with $[\eta^2\text{-}Te_2]^{2-}$ and $[Te]^{2-}$ ligands.[14,22a−c,23a−c,24] Further evidence for the switch between contact- and separated-ion pairs upon changing the solvent polarity comes from the NMR analysis of the uranium analogue, [K(18-crown-6)][U(η^2-Te_2)$(NR_2)_3$].[4h] For this complex, a single ^{1}H NMR peak for the 18-crown-6 moiety appears at its usual resonance frequency ($\delta(^1H)$ = 3.45 ppm) in pyridine-d_5, whereas in C_6D_6 it is paramagnetically shifted due to its close proximity to the U(IV) center (a contact-ion pair). Finally, Raman spectra of complexes **4** and **5** were also recorded (Figure S35); however, in neither case definitive Th=E stretching assignments could be made.

Electronic Structure Analysis. To explore the actinide-chalcogen (An−E) bonding more thoroughly, we investigated the electronic structures of the target compounds **2**−**5** using the Natural Bond Orbital (NBO),[25] Quantum Theory of Atoms-in-Molecules (QTAIM),[26] and Energy Decomposition Analysis (EDA)[27] approaches at the DFT level. For a reliable comparison and more complete picture (see analysis of NMR chemical shifts below), we also analyzed the electronic structures of the previously reported Th(IV) oxo and sulfido congeners,[6] as well as of their oxo-uranium(VI) homologues,[4i] using the same computational approach.

First, we note an excellent agreement between PBE0-D3(BJ)/def2-TZVP/ECP optimized and X-ray determined structural parameters, with differences in Th−E and Th−N bond lengths of less than 0.04 Å (cf. Tables 1 and 2). The average Th−E bond lengths in dichalcogenide complexes [K(18-crown-6)][Th(η^2-E_2)$(NR_2)_3$] (E = S, Se, Te) are comparable with those derived from the sum of single-bond covalent (or effective ionic) radii, while the Th−O bond distance in an analogous peroxide is shorter by ∼0.14 Å (Figure

DOI: 10.1021/jacs.5b07767
J. Am. Chem. Soc. 2016, 138, 814−825

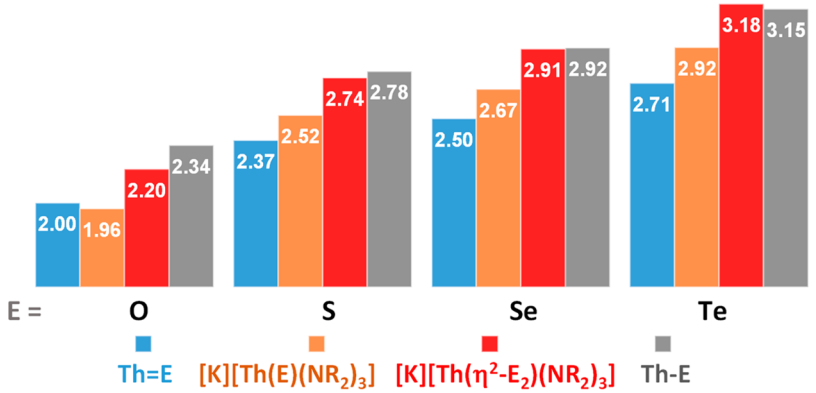

Figure 3. Optimized Th−E bond lengths (in Å) in mono- and dichalcogenide complexes $[K(18\text{-crown-}6)][Th(E_n)(NR_2)_3]$ (E = O, S, Se, Te; n = 1, 2) in comparison with those derived from the sum of double-bond covalent radii (data in blue) and effective ionic radii (data in gray).[17]

3). In contrast, the Th−E distances in the monochalcogenide series $[K(18\text{-crown-}6)][Th(E)(NR_2)_3]$ are considerably below the sum of corresponding single-bond covalent radii and lie slightly below (E = O) or above (E = S, Se, Te) the sum of double-bond covalent radii (cf. Figure 3), suggestive of the multiple bond character of the Th−E interaction. In addition, dissociation of cation/anion pairs in **2**−**5** (which occurs upon dissolution of these compounds in polar solvents, as indicated by NMR spectral data) results in further shortening of the Th−E distances (by ∼0.05 Å) and leads to a marginal increase of the Th−E bond-order (cf. Tables S2−S5 in Supporting Information for comparison of structural and bonding parameters for the contact- and separated-ion pairs complexes). Note that for consistent comparison with uranium complexes containing a different counterion, only anionic parts of the complexes are discussed below, if not stated otherwise.

For monochalcogenide complexes $[Th(E)(NR_2)_3]^-$ (and their K^+ adducts), NBO/NLMO analysis shows that the Th−E bond consists of three bonding pairs ($\sigma + 2\pi$ bonds) sharing six electrons in total in the Lewis structure notation (cf. Figure 4

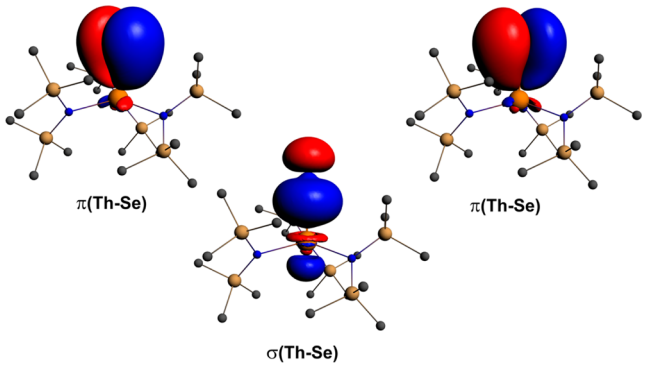

Figure 4. Th−Se ($\sigma + 2\pi$) bonding NLMOs in $[Th(Se)(NR_2)_3]^-$ (isosurface plots ±0.03 au; hydrogen atoms are omitted for clarity).

and Table 3 for the composition of the An−E bonding NLMOs). The cylindrical triple-bond symmetry of the Th−E interaction is also supported by zero ellipticities, ε, at the bond critical point (BCP) as indicated from QTAIM topological analysis (Table 4). In addition, all three Th−N bonds possess a partial double-bond character, evident also from a somewhat shorter Th−N bond distances as compared to the sum of single bond covalent radii (2.46 Å) and noncylindrical Th−N bond symmetry with the ellipticity values, ε, deviating substantially from zero (cf. Table 4). A similar NBO/NLMO picture is obtained for analogous $[U(O)(E)(NR_2)_3]^-$ complexes, which possess, however, an extra U≡O triple bond.[4i,28] In general, all the Th−E bonding NLMOs are predominantly localized on the chalcogen atom, with only a little thorium 5f orbital involvement in bonding (the overall contribution of Th(5f) orbitals to the σ(Th−E) bonding NLMO is ∼2%, while a somewhat larger contribution, 3−8%, is found for the π bonding NLMOs). A much more pronounced 5f orbital participation is identified in the uranium series, where the σ(U−E) bonding component has larger U(5f) atomic orbital contribution (14−24%) than the π(U−E) bonding component (12−15%). These findings closely corroborate our previous computational analyses of structurally related actinide-chalcogenide complexes.[4i,6]

According to natural population and QTAIM analysis, the An−E bonds in the studied complexes are strongly polar and exhibit an appreciable ionic character, more so for thorium than for uranium. The An−E bond becomes less polar as group 16 is descended, consistent with decreasing electronegativity of the chalcogen atoms (O > S > Se > Te) and decreasing polarization of the bonding NLMOs toward the E atom (cf. Table 3). The highly polar nature of the multiple An−E bond significantly reduces the formal covalent bond order of 3 to lower values, in accordance with the Th−E bond-length derived bond orders, which vary between ca. 1.5−2.0 (cf. Figure 3). The latter is also confirmed by the calculated QTAIM delocalization indices (DI) collected in Table 4. The DI integrates the electron density in the bonding region between two atoms in question and it is closely related to the bond order, noting that the computed values are always smaller than those expected from the Lewis structure (the difference between the formal bond multiplicity and the DI is often taken as a measure of bond polarity). The DI(Th−E) values within monochalcogenide series are twice as large as those in the corresponding dichalcogenide series, and DI(Th−Se) in $[Th(Se)(NR_2)_3]^-$ is ca. 2.8 higher than that calculated for the previously reported thorium selenate $[Th\{Se_2P(Ph)(OMe)\}_4]$[5c] (cf. Tables 4 and 5). This confirms a significant electron density accumulation in the Th−E bonding region of the title complexes.

Interestingly, when going from the hard oxo to soft E ligands ($E = S^{2-}$, Se^{2-}, Te^{2-}), the delocalization index for the An−E bond decreases, although the bond becomes less polar (cf. Tables 3 and 4). The opposite and thus chemically more intuitive trend (an increasing An−E bond order with decreasing bond polarity along the line O < S < Se < Te) is observed in

DOI: 10.1021/jacs.5b07767
J. Am. Chem. Soc. 2016, 138, 814−825

Table 3. NPA Atomic Charges and Compositions (%) of the An−E Bonding NLMOs in Chalcogenide Complexes $[Th(E)(NR_2)_3]^-$ and $[U(O)(E)(NR_2)_3]^-$ (E = O, S, Se, Te)[a]

	NPA charge		An−E bonding NLMOs[b,c]							
E	q(An)	q(E)		% An	An(s)	An(d)	An(f)	% E	E(s)	E(p)
$[Th(E)(NR_2)_3]^-$ (An = Th)										
O	1.86	−1.19	σ	6.9	9	69	22	93.0	90	10
			π	11.3	0	70	30	88.0	0	100
S	1.20	−0.72	σ	18.8	11	77	11	80.5	52	48
			π	18.5	0	67	33	80.2	0	99
Se	1.10	−0.62	σ	21.1	14	75	10	78.1	46	54
			π	19.8	0	65	35	78.8	0	99
Te	1.00	−0.54	σ	24.8	19	73	9	74.1	38	62
			π	20.3	0	62	38	78.0	0	100
$[U(O)(E)(NR_2)_3]^-$ (An = U)										
O	1.81	−0.66	σ	24.0	0	16	84	74.8	27	73
			π	19.9	0	39	61	79.7	0	100
S	1.08	−0.18	σ	31.5	7	49	44	68.5	26	74
			π	25.4	0	49	51	74.6	1	99
Se	1.01	−0.15	σ	35.8	4	29	68	62.4	22	78
			π	26.0	0	43	57	72.3	1	99
Te	1.02	−0.14	σ	38.4	6	30	64	59.5	19	81
			π	24.0	0	43	57	73.9	0	100

[a]PBE0/def2-TZVP/ECP results (cf. Computational Details). [b]The compositions are given for one σ and two π bonding NLMOs (for the latter, only one set is given, the second π(An−E)-type bonding NLMO has identical composition). [c]Note that Th(p) and U(p) contribution in An−E bonding is negligible, ranging from 0 to 2%.

Table 4. QTAIM Electron (ρ_b) and Energy (H_b) Densities (in au) and Ellipticities (ε) at the An−E and An−N Bond Critical Points in $[Th(E_n)(NR_2)_3]^-$ and $[U(O)(E)(NR_2)_3]^-$ (E = O, S, Se, Te; n = 1, 2) Complexes[a]

	An−E				An−N			
E	ρ_b	H_b	ε	DI	ρ_b	H_b	ε	DI
$[Th(\eta^2\text{-}E_2)(NR_2)_3]^-$[b]								
O	0.12	−0.04	0.13	0.699	0.08	−0.02	0.14	0.578
S	0.07	−0.02	0.08	0.652	0.08	−0.02	0.13	0.627
Se	0.06	−0.01	0.09	0.632	0.08	−0.02	0.13	0.645
Te	0.04	−0.01	0.09	0.599	0.09	−0.02	0.14	0.670
$[Th(E)(NR_2)_3]^-$								
O	0.21	−0.14	0.00	1.449	0.07	−0.02	0.11	0.558
S	0.10	−0.04	0.00	1.297	0.08	−0.02	0.14	0.633
Se	0.08	−0.03	0.00	1.266	0.08	−0.02	0.14	0.650
Te	0.07	−0.02	0.00	1.202	0.09	−0.02	0.14	0.674
$[U(O)(E)(NR_2)_3]^-$								
O	0.30	−0.26	0.00	1.834	0.09	−0.02	0.09	0.675
S	0.14	−0.07	0.00	1.729	0.10	−0.03	0.12	0.759
Se	0.11	−0.05	0.00	1.697	0.10	−0.03	0.12	0.782
Te	0.09	−0.03	0.00	1.669	0.11	−0.03	0.13	0.811

[a]Delocalization Indices (DI) as a measure of the bond covalency are given as well. PBE0/def2-TZVP/ECP results (cf. Computational Details). [b]For dichalcogenide complexes, only the average values over two An−E bonds are given.

homoleptic actinyl series ThE_2 and UE_2^{2+} (Table S6 in Supporting Information). The disproportion between the An−E bond polarity and the An−E bond order within the isoelectronic $[An(E)(NR_2)_3]^-$ series might be ascribed to the heterogeneous coordination environment around the metal center and can be rationalized by withdrawing the electron density from the multiple An−E bonds (E = S, Se, Te) by more electronegative nitrogen atoms of the NR_2^- ligands and accumulation of the electron density in the An−N bonding region (more so for less electronegative chalcogen atoms; the opposite holds for complexes with the oxo ligand). This is evident from DI values for An−E and An−N bonds, for which the trends go opposite upon changing the E atom (cf. Table 4). The same argument can be used to explain the An−N bond contraction as the chalcogen atom becomes less electronegative. This also indicates that results of natural population analysis are solely not enough to determine the degree of covalency for a particular metal−ligand bond in heteroleptic complexes. We note in passing that DI values in ThE_2 model series range from 1.71 to 1.95 and follow closely the Gopinathan-Jug bond orders[29] (cf. Table S6 in Supporting Information), showing that the title complexes are not far away from the maximal effective Th−E bond multiplicity, which is largely reduced by the intrinsic An−E bond polarity and can be further controlled by supporting ligands.

The other QTAIM topological indicators are also suggestive of a quite reduced An−E bond covalency, more so for thorium than for uranium (cf. Table 4). The accepted wisdom is that electron densities ρ_b at the BCP larger than 0.2 eÅ^{-3} indicate the covalent bond, while ρ_b < 0.1 eÅ^{-3} are typical for ionic interactions; the more stabilizing covalent interaction, the more negative energy density H_b.[26]

Although the QTAIM metrics at the BCP should be taken with some caution when comparing systems with substantially different bond lengths,[5c] the decreasing An−E bond covalency as the chalcogen atom becomes heavier, is also supported independently by the EDA analysis (cf. Table S7 in Supporting Information).

Analysis of NMR Chemical Shifts. During the past decade, DFT electronic structure analysis became a routine but powerful tool for exploring actinide-ligand bonding. However, apart from the X-ray data (which are not always available), the studies mostly rely on purely theoretical models and a bridge between the spectroscopic observables and the electron density (with its topology descriptors) is often missing.

DOI: 10.1021/jacs.5b07767
J. Am. Chem. Soc. 2016, 138, 814−825

Table 5. ^{77}Se and ^{125}Te NMR Chemical Shifts (δ in ppm vs Me_2Se and Me_2Te, Respectively) and Individual Isotropic Shielding Contributions (σ, in ppm) in Actinide Complexes with a Direct An−E Bonding Interaction[a]

Complex	DI	^{77}Se					DI	^{125}Te				
	An-Se	σ^d	σ^p	σ^{SO}	$\delta_{calcd.}$	$\delta_{expt.}$	An-Te	σ^d	σ^p	σ^{SO}	$\delta_{calcd.}$	$\delta_{expt.}$
$[Th\{E_2P(Ph)(OMe)\}_4]$	0.446	2976	−1487	201	224	222[b,f]	0.475	5311	−3068	700	509	[d]
[K(18-crown-6)][$Th(E_2)(NR_2)_3$] **2** (E = Se), **3** (E = Te)	0.529	2974	−1493	171	262	246[b]	0.494	5310	−2229	771	−402	−351[b]
$[Th(E_2)(NR_2)_3]^-$	0.632	2972	−1646	182	405	302[c]	0.599	5310	−2515	815	−160	−272[c]
[K(18-crown-6)][$Th(E)(NR_2)_3$] **4** (E = Se), **5** (E = Te)	1.057	2979	−1998	119	814	885[b]	0.991	5313	−2838	631	344	481[b]
$[Th(E)(NR_2)_3]^-$	1.266	2978	−2264	134	1066	992[c]	1.202	5313	−3263	682	719	628[c]
$[Pa(E)(NR_2)_3]$	1.620	2976	−3625	265	2298	[d]	1.613	5311	−5827	1045	2922	[d]
$[U(O)(E)(NR_2)_3]^-$	1.697	2979	−5858	386	4407	4905[e]	1.669	5311	−10974	1915	7199	[d]
$[U(NPh)(E)(NR_2)_3]^-$	1.706	2978	−6941	599	5277	[d]	1.659	5312	−13940	2743	9336	[d]
$[U(S)(E)(NR_2)_3]^-$	1.740	2979	−7724	772	5887	[d]	1.693	5313	−16771	3519	11390[g]	[d]
$[U(E)(Me)(NR_2)_3]$	1.808	2978	−8960	979	6917	[d]	1.804	5310	−22930	4923	16147[g]	[d]
$[U(E)(F)(NR_2)_3]$	1.874	2977	−9905	1126	7715	[d]	1.894	5310	−33596	6730	25006[g]	[d]
Me_2E (reference)		2975	−1232	171	0.0	0.0		5307	−2581	725	0.0	0.0

[a]Delocalization Indices (DI) of the An−E bonds are given as well. NMR chemical shieldings/shifts calculated at the 2c-ZORA(SO)/PBE0/TZ2P level in the gas-phase (cf. Computational Details). [b]Measured in C_6D_6. [c]Given complex (**2**−**5**) with $[K(18\text{-crown-6})]^+$ counterion measured in pyridine-d_5. [d]Model complex, experimental data not available. [e]$[CoCp^*_2][U(O)(Se)(NR_2)_3]$ measured in pyridine-d_5 (see ref 4i for the synthesis). [f]Data taken from ref 5c. [g]Extraordinarily high $\sigma^p(^{125}Te)/\delta(^{125}Te)$ values in some telluride complexes could be attributed to a low-lying triplet state, indicating instability of these molecules toward U(VI) reduction.

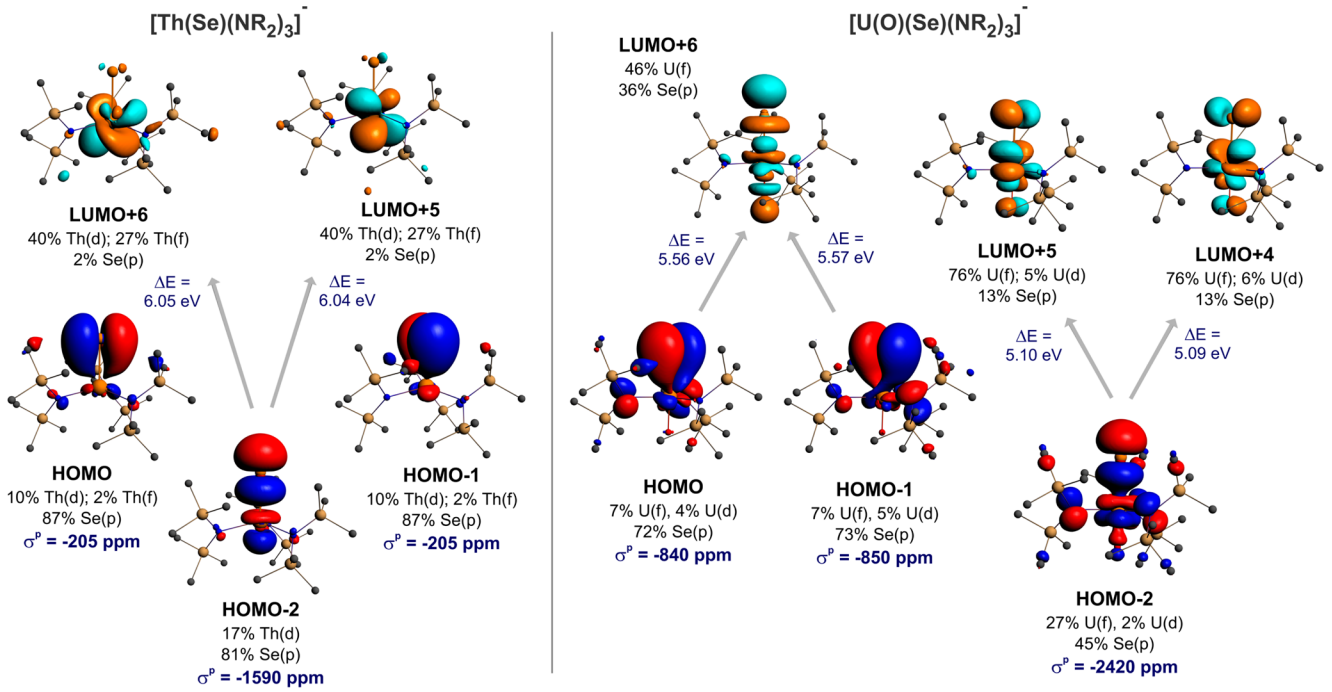

Figure 5. Isosurface plots (±0.035 au) of the dominant occupied and virtual MOs contributing to the isotropic σ^p (^{77}Se) value in thorium (left) and oxo-uranium (right) selenide complexes.

In this regard, ^{77}Se and ^{125}Te NMR chemical shifts in **2**−**5**, in the corresponding anions, and in the previously characterized $[Th\{Se_2P(Ph)(OMe)\}_4]$ complex, were calculated at the two-component ZORA-SO relativistic level including spin−orbit coupling, in conjunction with a PBE0 hybrid functional and TZ2P basis set (cf. Computational Details and Table 5). Excellent agreement between theoretical and experimental δ values validates the applicability of the chosen DFT method for in-depth analysis. Inclusion of bulk solvent effects (considering benzene as a solvent) affect the calculated NMR shifts in **2**−**5** only marginally (by less than 30 and 50 ppm for ^{77}Se and ^{125}Te, respectively), and the increase of solvent polarity when going from benzene (ε_r = 2.3) to pyridine (ε_r = 12.4) cannot solely explain the remarkable deshieldings observed in the latter solvent (cf. Table 5 and Table S8 in Supporting Information). This supports a complete or partial dissociation of the contact ion pairs in **2**−**5** in pyridine. To study the relationships between ^{77}Se and ^{125}Te NMR shifts, and the An−E bonding characteristics systematically, we extended the investigated series to several isoelectronic Pa(V) and U(VI) complexes (this results in a set of 22 actinide complexes, of which 10 were synthesized and characterized experimentally by NMR; cf. Table 5). In this regard, we also recorded the ^{77}Se NMR shift in our recently prepared $[CoCp^*_2][U(O)(Se)(NR_2)_3]$ complex.[4i]

DOI: 10.1021/jacs.5b07767
J. Am. Chem. Soc. 2016, 138, 814−825

In accordance with DFT predictions we have found for this complex an unprecedentedly high frequency resonance of ^{77}Se at 4905 ppm, which is to our best knowledge the most deshielded ^{77}Se shift reported so far for a diamagnetic substance. This extends the known ^{77}Se chemical shift range from ~3300 ppm to almost 6000 ppm (with the low-frequency extreme $\delta(^{77}\text{Se})$ = −900 ppm, reported for a selenium-bridged tungsten complex $[\text{CpW(CO)}_3]_2(\mu\text{-Se})$;[30] and the triselena-substituted aromatic dication[31] with $\delta(^{77}\text{Se})$ = +2434 ppm as the former extreme on the high-frequency side).[31] We note in passing that $\delta(^{125}\text{Te})$ of the telluride homologue $[\text{U(O)(Te)(NR}_2)_3]^-$ is also predicted to exceed the known chemical shift range of ^{125}Te, which is nearly 5000 ppm.[32]

To gain deeper insight into the observed trends, first we separate the calculated shieldings into the well-known diamagnetic (σ^d) and paramagnetic (σ^p) contributions, and into a spin−orbit (σ^{SO}) term (Table 5). Both, ^{77}Se and ^{125}Te NMR shift changes are dominated by the paramagnetic shielding, σ^p, which arises from symmetry-allowed mixing of ground and excited states and cause high-frequency (down-field) shifts in these complexes.[33] In contrast to our previous studies on unprecedentedly high-frequency ^{1}H and ^{13}C NMR shifts in some actinide hydride and alkyl complexes,[9] the spin−orbit(SO)-induced shielding, σ^{SO}, is comparatively small here and reaches up to 14% (^{77}Se) and 35% (^{125}Te) of σ^p in an absolute value, but with an opposite sign. This is not surprising as SO effects on the ^{77}Se and ^{125}Te shieldings belong to the HAHA effects (heavy-atom effects on the heavy-atom shielding), which are essentially atomic in nature and are largely canceled for relative NMR shift trends. However, σ^{SO} has a sizable contribution in absolute terms for chalcogen chemical shifts in some uranium(VI) complexes (shifting the resonance to somewhat lower frequencies) and it has to be considered to reproduce the experimental values quantitatively (more so for ^{125}Te than for ^{77}Se shifts).

According to Ramsey's formula,[34,35] σ^p is proportional to the overlap between magnetically coupled orbitals and it is inversely proportional to the cube of the radial expansion of the shielding electrons from the nucleus in question ($1/r^3$) and the energy separation between the corresponding occupied and virtual orbitals ($1/\Delta E$). The first two terms are related to bond covalency and atomic charges, which often leads to reasonable correlations of σ^p with these local properties, given that ΔE remains sufficiently constant within the studied series. Using the relativistic NMR shielding analysis method[36] (cf. Figure 5 and Tables S10 in SI for more data), it is shown that σ^p values for ^{77}Se and ^{125}Te nuclei in the studied $[\text{An(E)(L)(NR}_2)_3]^q$ (An = Th, Pa, U; L = −, O, NPh, S, Me, F; q = −1, 0) series arise from a few contributions, but there are only three which stand out by being larger and by differing more between the complexes. These correspond to excitations from the occupied σ(An−E) and π(An−E)-type bonding MOs, both consisting predominantly of chalcogen p atomic orbitals with some metal d and/or f character (Figure 5). Among them, the σ(An−E)-type HOMO−2 has the largest deshielding contribution and it is primarily coupled with vacant π antibonding MOs composed largely from actinide 6d and 5f-orbitals. Magnetic couplings between π(An−E) and σ^*(An−E)-type MOs contribute as well, whereby their overall deshielding contribution is ca. 20% in the thorium complexes, and they become almost equally important as the σ(An−E)-type bonding MO upon replacing the Th atom by uranium (Figure 5). On this basis, it might be anticipated that larger covalency of the An−E bond will enhance the overlap between magnetically coupled bonding MOs with vacant, predominantly metal-centered, orbitals and will thus cause the larger deshielding (high-frequency shift). This trend is already obvious when comparing the remarkable increase of both $\delta(^{77}\text{Se})$ and $\delta(^{125}\text{Te})$ values when going from the Th dichalcogenide complexes to their monochalcogenide counterparts (**2** → **4**, **3** → **5**), where the former possess much smaller Th−E bond covalency, as indicated by DI values (Table 4).

This finding encouraged us to establish a correlation between the chemical shifts of the chalcogenide ligands and the delocalization index of the Th−E bond.[37] Note that the correlation of chemical shifts instead of the σ^p term discussed above is more practical (δ is a directly measurable quantity) and well justified, as σ^d remains constant and changes in σ^{SO} go roughly parallel with the paramagnetic shielding in an absolute value (cf. Figure S38 in Supporting Information). Consistent with our hypothesis, a plot of the ^{77}Se (and ^{125}Te) chemical shifts for the contact- and separated-ion pairs of complexes **2** and **4** (**3** and **5**) vs their calculated DI(Th−E) values results in a linear relationship (Figure 6; see also Figures S36−S37). Importantly, upon forming the separated ion pairs of **2**-**5** we would anticipate a strengthening of the Th−Se and Th−Te interactions, which is exactly what is predicted by the DFT

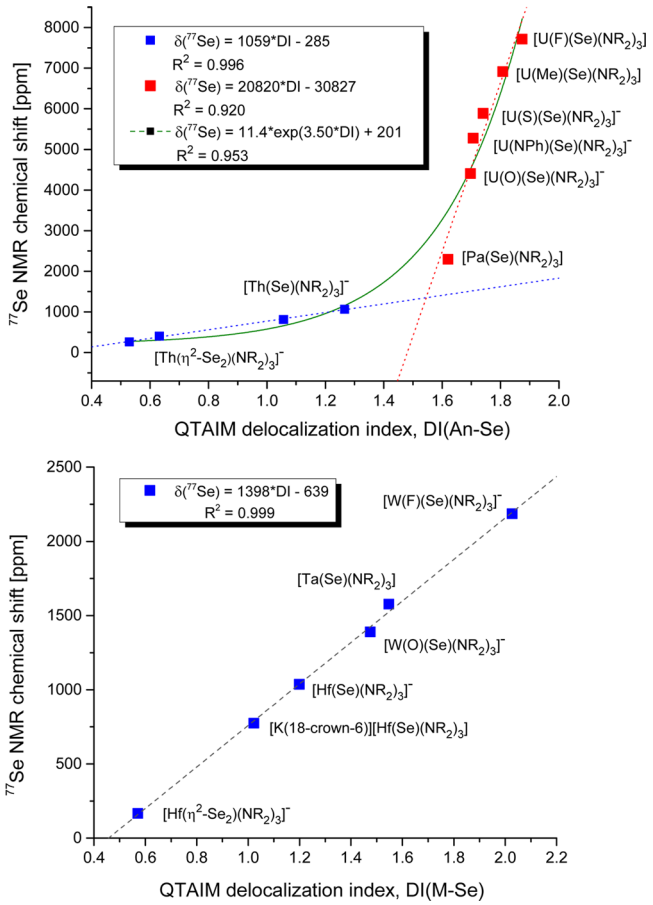

Figure 6. Correlation of calculated ^{77}Se NMR chemical shifts in actinide $[\text{An(Se)(L)(NR}_2)_3]^q$ series (upper) and their transition-metal homologues (lower) with QTAIM delocalization index of the An-Se and M-Se bond, respectively. See Table 5 and Table S9 for numerical data and Figure S37 in Supporting Information for the analogous correlations of ^{125}Te NMR shifts.

DOI: 10.1021/jacs.5b07767
J. Am. Chem. Soc. 2016, 138, 814−825

calculations (as evident from the DI values) and reflected by the more deshielded ^{77}Se and ^{125}Te chemical shifts.

In view of this finding for a limited series of Th chalcogenide complexes, we speculated that the relationship between ^{77}Se (and ^{125}Te) chemical shifts vs delocalization index of the An−E bond could be extended also to heavier actinides and transition-metal homologues. To explore this proposal, and to draw more general conclusions, we correlated computed ^{77}Se and ^{125}Te NMR shifts and delocalization indices of the An−E or M−E bonds for a large series of hypothetical complexes, which are isoelectronic with the title compounds (cf. Figure 6; for consistency with data of the hypothetical complexes, we used calculated NMR shifts also for Th complexes in these correlations). While there is a good linear relationship within the Th series, this correlation deviates substantially from linearity when including the heavier actinides. The resulting plot, however, demonstrates the enhanced deshielding with increasing covalency, and can be viewed as an exponential function or two discrete linear plots—one for Th complexes with only minor 5f-orbital involvement in the Th−E interaction and a second for Pa(V) and U(VI) complexes with an appreciable amount of actinide 5f orbital contribution to the An−E bonding. Besides increasing covalency, the An(5f) orbitals also cause a decrease of excitation energies when going from Th to heavier analogues, but the drop in the energy gap is too small to solely explain the dramatic increase of σ^{p}. Furthermore, variations in ΔE are comparable with those in the hypothetical transition-metal complexes $[M(Se)(L)(NR_2)_3]^q$ (M = Hf, Ta, W; L = −, O, F; q = −1, 0) (cf. Tables S10 and S11 in SI). The latter series, however, shows an excellent linear correlation between computed ^{77}Se NMR shifts and the delocalization index, DI(M-E) (cf. Figure 6), thus reinforcing the results of the shielding analysis and attributing the exponential increase of σ^{p} to a significant increase of 5f-orbitals participation in An−E bonding when going from Th to U (cf. Table 3).

CONCLUSION

In summary, we have synthesized the thorium selenide and telluride coordination complexes, $[K(18\text{-crown-6})][Th(E)(NR_2)_3]$ (E = Se, Te), which represent the first reported molecular thorium selenide and tellurides, respectively. These complexes feature the shortest known Th−Se and Th−Te distances, which are suggestive of multiple bond character. The natural bond analysis and QTAIM metrics show that $[Th(E)(NR_2)_3]^-$ (E = O, S, Se, Te) complexes contain a Th≡E triple (σ+2π) bond, which is strongly polarized toward the chalcogen atom. ^{77}Se and ^{125}Te NMR chemical shifts of chalcogenide ligands within the isostructural $[An(E)(L)(NR_2)_3]^q$ series are found to correlate with the An−E bond delocalization index, as a measure of the bond covalency, and actinide 5f orbital participation. Although these two factors are intimately interconnected within the actinide complexes (which hampers the establishment of one-parameter linear correlations between ^{77}Se/^{125}Te chemical shifts and the corresponding atomic charges or An−E bond orders across the entire actinide series), these NMR chemical shifts provide valuable insight into the actinide-chalcogen bonding, particularly when combined with detailed quantum-chemical analysis of these spectroscopic observables. Most importantly, our pilot analysis allows for examination of the covalency/ionicity of actinide-ligand bonds by NMR spectroscopy, and demonstrates the utility of this approach for exploring the electronic structure of actinide and transition-metal chalcogenide complexes.

EXPERIMENTAL SECTION

General Methods. All reactions and subsequent manipulations were performed under anaerobic and anhydrous conditions under an atmosphere of nitrogen. Hexanes, Et_2O, tetrahydrofuran (THF), and toluene were dried using a Vacuum Atmospheres DRI-SOLV Solvent Purification system and stored over 3 Å sieves for 24 h prior to use. Benzene-d_6 and pyridine-d_5 were dried over 3 Å molecular sieves for 24 h prior to use. $[Th(I)(NR_2)_3]$,[6] $[K(18\text{-crown-6})]_2[Se_4]$,[4h] $[K(18\text{-crown-6})]_2[Te_2]$,[4h] and $[CoCp^*_2][U(O)(Se)(NR_2)_3]$,[4i] were synthesized according to the previously reported procedures. Thorium(IV) nitrate hydrate was purchased from Strem Chemicals, while elemental Se, elemental Te, and $NaNR_2$ were purchased from Acros Organics. Unless noted, all reagents were used as received.

NMR spectra were recorded on a Varian UNITY INOVA 400 MHz spectrometer, a Varian UNITY INOVA 500 MHz spectrometer, a Varian UNITY INOVA 600 MHz spectrometer, or an Agilent Technologies 400-MR DD2 400 MHz spectrometer. ^{1}H NMR spectra were referenced to external $SiMe_4$ using the residual protio solvent peaks as internal standards. ^{13}C{^{1}H}, ^{31}P{^{1}H}, ^{77}Se{^{1}H}, and ^{125}Te{^{1}H} NMR spectra were referenced indirectly with the ^{1}H resonance of $SiMe_4$ at 0 ppm, according to IUPAC standard,[38] using the residual solvent peaks as internal standards. ^{77}Se and ^{125}Te NMR spectra were recorded at an operating frequency of 76.28 and 126.20 MHz, respectively. IR spectra were recorded on a Nicolet 6700 FT-IR spectrometer. Raman spectra were recorded on a LabRam Aramis microRaman system (Horiba Jobin Yvon) equipped with 1200 grooves/mm holographic gratings, and Peltier-cooled CCD camera. The 633 nm ouput of a Melles Griot He−Ne laser was used to excite the samples, which were collected in a back scattering geometry using a confocal Raman Microscope (high stability BX40) equipped with Olympus objectives (MPlan 50x). Sample preparation was performed inside the glovebox: Pure crystalline solid samples were placed between a glass microscope slide and coverslip, sealed with a bead of silicone grease, and removed from the glovebox for spectral acquisition. Elemental analyses were performed by the Micro-Analytical Facility at the University of California, Berkeley.

X-ray Crystallography. Data for **2**, **3**, **4**, and **5** were collected on a Bruker KAPPA APEX II diffractometer equipped with an APEX II CCD detector using a TRIUMPH monochromator with a Mo Kα X-ray source (α = 0.71073 Å). The crystals were mounted on a cryoloop under Paratone-N oil, and all data were collected at 100(2) K using an Oxford nitrogen gas cryostream. Data were collected using ω scans with 0.5° frame widths. Frame exposures of 20 s were used for **2**. Frame exposures of 5 s were used for **3** and **4**. Frame exposures of 10 s were used for **5**. Data collection and cell parameter determination were conducted using the SMART program.[39] Integration of the data frames and final cell parameter refinement were performed using SAINT software.[40] Absorption correction of the data was carried out using the multiscan method SADABS.[41] Subsequent calculations were carried out using SHELXTL.[42] Structure determination was done using direct or Patterson methods and difference Fourier techniques. All hydrogen atom positions were idealized, and rode on the atom of attachment. Structure solution, refinement, graphics, and creation of publication materials were performed using SHELXTL.[42]

The diethyl ether solvate molecule in complexes **2** and **3** exhibited positional disorder. One carbon atom was modeled over two positions in a 50:50 ratio. The C−C and C−O bond distances of the diethyl ether solvate were constrained to 1.54 and 1.45 Å, respectively, using the DFIX command. The Th and Te atoms of complex **5** exhibited positional disorder and were modeled over two positions in a 90:10 ratio. In addition, the anisotropic displacement parameters of the Th, Te, K, Si, O, N, and C atoms among the four molecules in the asymmetric unit were constrained with the EADP command. Two of the diethyl ether solvate molecules in **5** exhibited positional disorder; one carbon of each molecule was modeled over two positions in a 50:50 ratio. The C−C and C−O bond distances of the diethyl ether

DOI: 10.1021/jacs.5b07767
J. Am. Chem. Soc. 2016, 138, 814−825

solvates were constrained to 1.54 and 1.45 Å, respectively, using the DFIX command. Hydrogen atoms were not assigned to disordered carbon atoms. A summary of relevant crystallographic data for **2**-**5** is presented in Table S1 in Supporting Information.

*Synthesis of [K(18-crown-6)][Th(Se$_2$)(NR$_2$)$_3$] (**2**).* To a colorless, cold (−25 °C), stirring mixure of [Th(I)(NR$_2$)$_3$] (40.7 mg, 0.048 mmol) in THF (3 mL) was added [K(18-crown-6)]$_2$[Se$_4$] (47.9 mg, 0.052 mmol). The color of the solution became pale orange upon addition. This mixture was allowed to stir for 20 min, whereupon the deposition of a black precipitate was observed. This mixture was filtered through a Celite column supported on glass wool (0.5 cm × 3 cm) to afford an orange solution. The solvent was then removed in vacuo to afford an orange solid. The solid was triturated with pentane (2 mL) to afford an orange powder. This powder was extracted with diethyl ether (5 mL) and filtered through a Celite column supported on glass wool (0.5 cm × 3 cm) to afford an orange solution. The volume of the filtrate was reduced to 2 mL in vacuo, and then the solution was transferred to a 4 mL scintillation vial that was placed inside a 20 mL scintillation vial. Toluene (6 mL) was then added to the outer vial. Storage of this two vial system at −25 °C for 48 h resulted in the deposition of an orange crystalline solid, which was isolated by decanting the supernatant (37.0 mg, 63%). Anal. Calcd for $C_{30}H_{78}KN_3O_6Se_2Si_6Th{\cdot}0.5C_4H_{10}O$: C, 31.72; H, 6.91; N, 3.47. Found: C, 31.38; H, 6.64; N, 3.27. ^{1}H NMR (400 MHz, 25 °C, benzene-d_6): δ 0.74 (s, 54H, NSiCH_3), 3.17 (s, 24H, 18-crown-6). ^{13}C{^{1}H} NMR (100 MHz, 25 °C, benzene-d_6): δ 6.05 (NSiCH_3), 70.18 (18-crown-6). ^{77}Se{^{1}H} (76.28 MHz, 25 °C, benzene-d_6): δ 246 (s, $\nu_{1/2}$ = 8 Hz). ^{1}H NMR (400 MHz, 25 °C, pyridine-d_5): δ 0.74 (s, 54H, NSiCH_3), 3.47 (s, 24H, 18-crown-6). ^{13}C{^{1}H} NMR (100 MHz, 25 °C, pyridne-d_5): δ 6.56 (NSiCH_3), 70.87 (18-crown-6). ^{77}Se{^{1}H} (76.28 MHz, 25 °C, pyridine-d_5): δ 302 (s, $\nu_{1/2}$ = 9 Hz). IR (KBr pellet, cm^{-1}): 608 (m), 665 (m), 774 (m), 847 (s), 930 (s), 964 (m), 1020 (w), 1057 (w), 1112 (s), 1182 (w), 1250 (s), 1284 (w), 1351 (m), 1400 (w), 1453 (w), 1472 (w).

*Synthesis of [K(18-crown-6)][Th(Se)(NR$_2$)$_3$] (**4**).* To an orange, cold (−25 °C), stirring solution of **2** (136.7 mg, 0.12 mmol) in diethyl ether (4 mL) was added Et$_3$P (18 μL, 0.12 mmol). The color of this solution became light yellow upon addition. This solution was allowed to stir for 90 min, whereupon the deposition of a white precipitate was observed. This mixture was then filtered through a Celite column supported on glass wool (0.5 cm × 3 cm) to afford a light yellow solution. The volume of this filtrate was reduced to 2 mL in vacuo. Storage of this solution at −25 °C for 24 h resulted in the deposition of an off-white solid, subsequently identified as Et$_3$P=Se by ^{31}P{^{1}H} and ^{77}Se{^{1}H} NMR spectroscopies (19.7 mg, 97%).[13] The solid was isolated by decanting the supernatant. The volume of the supernatant was reduced in vacuo to 1 mL. This solution was then transferred to a 4 mL scintillation vial that was placed inside a 20 mL scintillation vial. Toluene (6 mL) was then added to the outer vial. Storage of this two vial system at −25 °C for 48 h resulted in the deposition of colorless crystals, which were isolated by decanting off the supernatant (28.8 mg, 22%). The supernatant was then transferred to a 4 mL scintillation vial that was placed inside a 20 mL scintillation vial. Toluene (6 mL) was then added to the outer vial. Storage of this two vial system at −25 °C for 48 h resulted in the deposition of additional colorless crystals. Total yield: 67.8 mg, 53%. Anal. Calcd for $C_{30}H_{78}KN_3O_6SeSi_6Th$: C, 32.89; H, 7.18; N, 3.84. Found: C, 33.20; H, 7.28; N, 4.00. ^{1}H NMR (400 MHz, 25 °C, benzene-d_6): δ 0.76 (s, 54H, NSiCH_3), 3.17 (s, 24H, 18-crown-6). ^{13}C{^{1}H} NMR (100 MHz, 25 °C, benzene-d_6): δ 5.75 (NSiCH_3), 70.11 (18-crown-6). ^{77}Se{^{1}H} (76.28 MHz, 25 °C, benzene-d_6): δ 885 (s, $\nu_{1/2}$ = 10 Hz). ^{1}H NMR (400 MHz, 25 °C, pyridine-d_5): δ 0.75 (s, 54H, NSiCH_3), 3.53 (s, 24H, 18-crown-6). ^{13}C{^{1}H} NMR (100 MHz, 25 °C, pyridine-d_5): δ 6.31 (NSiCH_3), 70.01 (18-crown-6). ^{77}Se{^{1}H} (76.28 MHz, 25 °C, pyridine-d_5): δ 992 (s, $\nu_{1/2}$ = 16 Hz). IR (KBr pellet, cm^{-1}): 500 (w), 606 (m), 667 (m), 758 (m), 771 (m), 836 (s), 843 (s), 862 (s), 1111 (s), 1182 (w), 1250 (s), 1285 (w), 1352 (m), 1402 (w), 1454 (w), 1474 (w). Raman (neat solid, cm^{-1}): 179 (m), 253 (m), 570 (m), 622 (m), 674 (m), 750 (w), 833 (m), 874 (w), 1145 (w), 1250 (w), 1277 (w), 1413 (w), 1478 (m).

*Synthesis of [K(18-crown-6)][Th(Te$_2$)(NR$_2$)$_3$] (**3**).* To a colorless, cold (−25 °C), stirring mixture of [Th(I)(NR$_2$)$_3$] (102.4 mg, 0.12 mmol) in diethyl ether (4 mL) was added [K(18-crown-6)]$_2$[Te$_2$] (106.9 mg, 0.12 mmol). The color of the solution became green upon addition. This mixture was allowed to stir for 30 min, whereupon the deposition of a black precipitate was observed. This mixture was then filtered through a Celite column supported on glass wool (0.5 cm × 3 cm) to afford a green solution. The volume of the filtrate was reduced to 1 mL in vacuo. Storage of this solution at −25 °C for 24 h resulted in the deposition of green crystals, which were isolated by decanting off the supernatant (58.2 mg, 36%). Anal. Calcd for $C_{30}H_{78}KN_3O_6Si_6Te_2Th{\cdot}0.5C_4H_{10}O$: C, 29.37; H, 6.39; N, 3.21. Found: C, 29.78; H, 6.34; N, 3.06. ^{1}H NMR (400 MHz, 25 °C, benzene-d_6): δ 0.79 (s, 54H, NSiCH_3), 3.14 (s, 24H, 18-crown-6). ^{13}C{^{1}H} NMR (100 MHz, 25 °C, benzene-d_6): δ 6.28 (NSiCH_3), 70.13 (18-crown-6). ^{125}Te{^{1}H} NMR (126.20 MHz, 25 °C, benzene-d_6): δ −351 (s, $\nu_{1/2}$ = 16 Hz). ^{1}H NMR (400 MHz, 25 °C, pyridine-d_5): δ 0.76 (s, 54H, NSiCH_3), 3.58 (s, 24H, 18-crown-6). ^{13}C{^{1}H} NMR (100 MHz, 25 °C, pyridine-d_5): δ 6.74 (NSiCH_3), 71.18 (18-crown-6). ^{125}Te{^{1}H} NMR (126.20 MHz, 25 °C, pyridine-d_5): δ −272 (s, $\nu_{1/2}$ = 28 Hz). IR (KBr pellet, cm^{-1}): 610 (m), 664 (m), 687 (m), 760 (m), 773 (m), 844 (s), 900 (s), 919 (s), 964 (m), 1059 (w), 1110 (s), 1183 (w), 1249 (s), 1283 (w), 1351 (m), 1454 (w), 1472 (w).

*Synthesis of [K(18-crown-6)][Th(Te)(NR$_2$)$_3$] (**5**).* To a green, cold (−25 °C), stirring solution of **3** (43.3 mg, 0.034 mmol) in diethyl ether (3 mL) was added Et$_3$P (30 μL, 0.20 mmol) and Hg (737.5 mg, 3.67 mmol). This mixture was allowed to stir for 24 h, whereupon the color of the solution bleached to colorless, concomitant with the deposition of a black precipitate. This mixture was filtered through a Celite column supported on glass wool (0.5 cm × 3 cm) to afford a colorless solution. The volatiles were then removed in vacuo to give a colorless solid (31.4 mg, 78%). Crystals suitable for X-ray crystallographic analysis were grown from a concentrated Et$_2$O solution stored at −25 °C for 24 h. Anal. Calcd for $C_{30}H_{78}KN_3O_6Si_6TeTh$: C, 31.49; H, 6.87; N, 3.67. Found: C, 31.66, H, 7.03, N, 3.52. ^{1}H NMR (400 MHz, 25 °C, benzene-d_6): δ 0.81 (s, 54H, NSiCH_3), 3.15 (s, 24H, 18-crown-6). ^{13}C{^{1}H} NMR (100 MHz, 25 °C, benzene-d_6): δ 6.45 (NSiCH_3), 70.16 (18-crown-6). ^{125}Te NMR (126.20 MHz, 25 °C, benzene-d_6): δ 481 (s, $\nu_{1/2}$ = 60 Hz). ^{1}H NMR (400 MHz, 25 °C, pyridine-d_5): δ 0.81 (s, 54H, NSiCH_3), 3.47 (s, 24H, 18-crown-6). ^{13}C{^{1}H} NMR (100 MHz, 25 °C, pyridine-d_5): δ 6.95 (NSiCH_3), 70.89 (18-crown-6). ^{125}Te NMR (126.20 MHz, 25 °C, pyridine-d_5): δ 628 (s, $\nu_{1/2}$ = 70 Hz). IR (KBr pellet, cm^{-1}): 609 (m), 664 (m), 687 (m), 759 (m), 773 (m), 837 (s), 930 (s), 963 (s), 1110 (s), 1181 (w), 1251 (s), 1285 (w), 1352 (m), 1454 (w), 1474 (w). Raman (neat solid, cm^{-1}): 176 (s), 260 (w), 280 (w), 388 (m), 627 (s), 676 (m), 747 (w), 791 (w), 835 (m), 876 (m), 1007 (w), 1143 (w), 1252 (m), 1277 (m), 1412 (m), 1476 (m).

Computational Details. All investigated structures were fully optimized at the PBE0 level of theory,[43] including an atom-pairwise correction for dispersion forces via Grimme's D3 model[44] with Becke-Johnson (BJ)[45] damping in the Turbomole program.[46] Quasirelativistic energy-consistent small-core pseudopotentials (effective-core potentials, ECP)[47] were used for the metal centers, with (8s7p6d1f)/[6s4p3d1f] and (14s13p10d8f1g)/[10s9p5d4f1g] Gaussian-type orbital valence basis sets for the transition-metal and actinide atoms, respectively. Ligand atoms were treated with an all-electron def2-TZVP basis set.[48] Relativistic all-electron DFT calculations of the nuclear shieldings were performed using the Amsterdam Density Functional (ADF) program suite,[49] employing the PBE0 exchange-correlation functional in conjunction with Slater-type orbital basis sets of triple-ζ doubly polarized (TZ2P) quality and an integration accuracy of 5. Both scalar and spin−orbit relativistic effects were treated by the two-component zeroth-order regular approximation (ZORA).[50] The calculated NMR shieldings have been broken down into MO contributions using the analysis tools in the ADF code. Bulk solvent effects in selected complexes were simulated by the conductor-like screening model (COSMO) as implemented self-consistently in ADF.[51] The computed ^{77}Se and ^{125}Te nuclear shieldings were converted to chemical shifts (δ, in ppm) relative to the shieldings of

DOI: 10.1021/jacs.5b07767
J. Am. Chem. Soc. 2016, 138, 814−825

Me_2Se and Me_2Te, respectively, computed at the same level (in the case of dichalcogenide complexes, the shifts were averaged over the chemically equivalent nuclei).

Natural population analyses (NPA) and analysis of natural localized molecular orbitals (NLMOs)[25] were carried out at the PBE0/def2-TZVP/ECP level using the NBO6 code, interfaced with Gaussian 09.[52,53] Bader's quantum theory of atoms-in-molecules (QTAIM)[26] analyses of the Kohn−Sham wave functions (generated in Gaussian at the same level as used for NLMO analysis and stored as .wfx files) were performed using the Multiwfn program.[54] The actinide-ligand bond covalency was also studied using a quantitative energy decomposition analysis (EDA) of the total bonding energy into electrostatic interaction, Pauli-repulsive orbital interactions and attractive orbital interactions, as implemented in the ADF code.[49,55]

■ ASSOCIATED CONTENT

Supporting Information

The Supporting Information is available free of charge on the ACS Publications website at DOI: 10.1021/jacs.5b07767.

X-ray crystallographic details. (CIF)

NMR, IR and Raman spectra for complexes **2**−**5**, more detailed quantum-chemical analysis of the An−E bonding and of $^{77}Se/^{125}Te$ NMR shieldings in the title Th chalcogenides and the related actinide and transition-metal complexes. (PDF)

■ AUTHOR INFORMATION

Corresponding Authors

*peter.hrobarik@tu-berlin.de

*hayton@chem.ucsb.edu

Notes

The authors declare no competing financial interest.

■ ACKNOWLEDGMENTS

This work was supported by the U.S. Department of Energy, Office of Basic Energy Sciences, Chemical Sciences, Biosciences, and Geosciences Division under Contract No. DE-SC-0001861. P.H. acknowledges support from the Berlin DFG excellence cluster on Unifying Concepts in Catalysis (UniCat).

■ REFERENCES

(1) (a) Burns, C. J. *Science* **2005**, *309*, 1823. (b) Hayton, T. W. *Chem. Commun.* **2013**, *49*, 2956. (c) Hayton, T. W. *Dalton Trans.* **2010**, *39*, 1145. (d) Jones, M. B.; Gaunt, A. J. *Chem. Rev.* **2013**, *113*, 1137.

(2) (a) Zi, G. *Sci. China: Chem.* **2014**, *57*, 1064. (b) King, D. M.; Liddle, S. T. *Coord. Chem. Rev.* **2014**, *266-267*, 2. (c) Neidig, M. L.; Clark, D. L.; Martin, R. L. *Coord. Chem. Rev.* **2013**, *257*, 394. (d) Kaltsoyannis, N. *Inorg. Chem.* **2013**, *52*, 3407.

(3) (a) Anderson, N. H.; Odoh, S. O.; Yao, Y.; Williams, U. J.; Schaefer, B. A.; Kiernicki, J. J.; Lewis, A. J.; Goshert, M. D.; Fanwick, P. E.; Schelter, E. J.; Walensky, J. R.; Gagliardi, L.; Bart, S. C. *Nat. Chem.* **2014**, *6*, 919. (b) Schmidt, A.-C.; Heinemann, F. W.; Maron, L.; Meyer, K. *Inorg. Chem.* **2014**, *53*, 13142. (c) Kosog, B.; La Pierre, H. S.; Heinemann, F. W.; Liddle, S. T.; Meyer, K. *J. Am. Chem. Soc.* **2012**, *134*, 5284. (d) Fortier, S.; Kaltsoyannis, N.; Wu, G.; Hayton, T. W. *J. Am. Chem. Soc.* **2011**, *133*, 14224. (e) King, D. M.; Tuna, F.; McInnes, E. J. L.; McMaster, J.; Lewis, W.; Blake, A. J.; Liddle, S. T. *Science* **2012**, *337*, 717. (f) King, D. M.; Tuna, F.; McInnes, E. J. L.; McMaster, J.; Lewis, W.; Blake, A. J.; Liddle, S. T. *Nat. Chem.* **2013**, *5*, 482. (g) Lu, E.; Cooper, O. J.; McMaster, J.; Tuna, F.; McInnes, E. J. L.; Lewis, W.; Blake, A. J.; Liddle, S. T. *Angew. Chem., Int. Ed.* **2014**, *53*, 6696. (h) Gardner, B. M.; Balázs, G.; Scheer, M.; Tuna, F.; McInnes, E. J. L.; McMaster, J.; Lewis, W.; Blake, A. J.; Liddle, S. T. *Angew. Chem., Int. Ed.* **2014**, *53*, 4484. (i) King, D. M.; McMaster, J.; Tuna, F.; McInnes, E. J. L.; Lewis, W.; Blake, A. J.; Liddle, S. T. *J. Am. Chem. Soc.* **2014**, *136*, 5619.

(4) (a) Brown, J. L.; Wu, G.; Hayton, T. W. *Organometallics* **2013**, *32*, 1193. (b) Camp, C.; Antunes, M. A.; Garcia, G.; Ciofini, I.; Santos, I. C.; Pecaut, J.; Almeida, M.; Marcalo, J.; Mazzanti, M. *Chem. Sci.* **2014**, *5*, 841. (c) Matson, E. M.; Goshert, M. D.; Kiernicki, J. J.; Newell, B. S.; Fanwick, P. E.; Shores, M. P.; Walensky, J. R.; Bart, S. C. *Chem. - Eur. J.* **2013**, *19*, 16176. (d) Franke, S. M.; Heinemann, F. W.; Meyer, K. *Chem. Sci.* **2014**, *5*, 942. (e) Lam, O. P.; Heinemann, F. W.; Meyer, K. *Chem. Sci.* **2011**, *2*, 1538. (f) Smiles, D. E.; Wu, G.; Hayton, T. W. *Inorg. Chem.* **2014**, *53*, 12683. (g) Smiles, D. E.; Wu, G.; Hayton, T. W. *J. Am. Chem. Soc.* **2014**, *136*, 96. (h) Smiles, D. E.; Wu, G.; Hayton, T. W. *Inorg. Chem.* **2014**, *53*, 10240. (i) Brown, J. L.; Fortier, S.; Wu, G.; Kaltsoyannis, N.; Hayton, T. W. *J. Am. Chem. Soc.* **2013**, *135*, 5352. (j) Brown, J. L.; Fortier, S.; Lewis, R. A.; Wu, G.; Hayton, T. W. *J. Am. Chem. Soc.* **2012**, *134*, 15468. (k) Ventelon, L.; Lescop, C.; Arliguie, T.; Leverd, P. C.; Lance, M.; Nierlich, M.; Ephritikhine, M. *Chem. Commun.* **1999**, 659.

(5) (a) Ren, W.; Zi, G.; Fang, D.-C.; Walter, M. D. *J. Am. Chem. Soc.* **2011**, *133*, 13183. (b) Ren, W.; Song, H.; Zi, G.; Walter, M. D. *Dalton Trans.* **2012**, *41*, 5965. (c) Behrle, A. C.; Barnes, C. L.; Kaltsoyannis, N.; Walensky, J. R. *Inorg. Chem.* **2013**, *52*, 10623. (d) Ren, W.; Zi, G.; Walter, M. D. *Organometallics* **2012**, *31*, 672. (e) Haskel, A.; Straub, T.; Eisen, M. S. *Organometallics* **1996**, *15*, 3773. (f) Bell, N. L.; Maron, L.; Arnold, P. L. *J. Am. Chem. Soc.* **2015**, *137*, 10492.

(6) Smiles, D. E.; Wu, G.; Kaltsoyannis, N.; Hayton, T. W. *Chem. Sci.* **2015**, *6*, 3891.

(7) (a) Behrle, A. C.; Levin, J. R.; Kim, J. E.; Drewett, J. M.; Barnes, C. L.; Schelter, E. J.; Walensky, J. R. *Dalton Trans.* **2015**, *44*, 2693. (b) Ren, W.; Zi, G.; Walter, M. D. *Organometallics* **2012**, *31*, 672.

(8) *Cambridge Structural Database (CSD, version 1.17)*; Cambridge Crystallographic Data Centre: Cambridge, U.K., 2014.

(9) (a) Hrobárik, P.; Hrobáriková, V.; Greif, A. H.; Kaupp, M. *Angew. Chem., Int. Ed.* **2012**, *51*, 10884. (b) Seaman, L. A.; Hrobárik, P.; Schettini, M. F.; Fortier, S.; Kaupp, M.; Hayton, T. W. *Angew. Chem., Int. Ed.* **2013**, *52*, 3259.

(10) See also our study on unusually large spin-orbit effects on ^1H NMR shifts in transition-metal hydride complexes: Hrobárik, P.; Hrobáriková, V.; Meier, F.; Repiský, M.; Komorovský, S.; Kaupp, M. *J. Phys. Chem. A* **2011**, *115*, 5654.

(11) For recent studies, see, e.g.: (a) Szabo, Z.; Grenthe, I. *Inorg. Chem.* **2010**, *49*, 4928. (b) Sutrisno, A.; Terskikh, V. V.; Huang, Y. *Chem. Commun.* **2009**, 186. (c) Laskowski, R.; Blaha, P. *J. Phys. Chem. C* **2015**, *119*, 731. (d) Martel, L.; Magnani, N.; Vigier, J. F.; Boshoven, J.; Selfslag, C.; Farnan, I.; Griveau, J. C.; Somers, J.; Fanghanel, T. *Inorg. Chem.* **2014**, *53*, 6928. (e) Merle, N.; Trébosc, J.; Baudouin, A.; Del Rosal, I.; Maron, L.; Szeto, K.; Genelot, M.; Mortreux, A.; Taoufik, M.; Delevoye, L.; Gauvin, R. M. *J. Am. Chem. Soc.* **2012**, *134*, 9263. (f) Mayer, F.; Platas-Iglesias, C.; Helm, L.; Peters, J. A.; Djanashvili, K. *Inorg. Chem.* **2012**, *51*, 170.

(12) (a) Brunner, H.; Kubicki, M.; Leblanc, J.-C.; Meier, W.; Moïse, C.; Sadorge, A.; Stubenhofer, B.; Wachter, J.; Wanninger, R. *Eur. J. Inorg. Chem.* **1999**, *1999*, 843. (b) Howard, W. A.; Parkin, G.; Rheingold, A. L. *Polyhedron* **1995**, *14*, 25. (c) Seikel, E.; Oelkers, B.; Sundermeyer, J. *Inorg. Chem.* **2012**, *51*, 2709. (d) Howard, W. A.; Trnka, T. M.; Parkin, G. *Organometallics* **1995**, *14*, 4037.

(13) Kuhn, N.; Henkel, G.; Schumann, H.; Frohlich, R. *Z. Naturforsch., B: J. Chem. Sci.* **1990**, *45*, 1010.

(14) Shin, J. H.; Parkin, G. *Organometallics* **1994**, *13*, 2147.

(15) Capps, K. B.; Wixmerten, B.; Bauer, A.; Hoff, C. D. *Inorg. Chem.* **1998**, *37*, 2861.

(16) D'Eye, R. W. M. *J. Chem. Soc.* **1953**, 1670.

(17) (a) Shannon, R. D. *Acta Crystallogr., Sect. A: Cryst. Phys., Diffr., Theor. Gen. Crystallogr.* **1976**, *A32*, 751. (b) Pyykkö, P. *J. Phys. Chem. A* **2015**, *119*, 2326.

(18) Wu, E. J.; Pell, M. A.; Ibers, J. A. *J. Alloys Compd.* **1997**, *255*, 106.

(19) Rocker, F.; Tremel, W. *Z. Anorg. Allg. Chem.* **2001**, *627*, 1305.

(20) Tougait, O.; Potel, M.; Noël, H. *Inorg. Chem.* **1998**, *37*, 5088.

DOI: 10.1021/jacs.5b07767
J. Am. Chem. Soc. 2016, 138, 814−825

(21) (a) D'Eye, R. W. M.; Sellman, P. G. *J. Chem. Soc.* **1954**, 3760. (b) Hahn, H.; Stocks, K. *Naturwissenschaften* **1968**, *55*, 389. (c) Hulliger, F. *J. Less-Common Met.* **1968**, *16*, 113. (d) Benz, R.; Zachariasen, W. H. *Acta Crystallogr., Sect. B: Struct. Crystallogr. Cryst. Chem.* **1970**, *26*, 823. (e) Beck, H. P.; Dausch, W. *Z. Anorg. Allg. Chem.* **1989**, *571*, 162. (f) Cody, J. A.; Ibers, J. A. *Inorg. Chem.* **1996**, *35*, 3836. (g) Narducci, A. A.; Ibers, J. A. *Inorg. Chem.* **1998**, *37*, 3798.

(22) (a) Piers, W. E.; Ziegler, T.; Fischer, J. M.; Macgillivray, L. R.; Zaworotko, M. J. *Chem. - Eur. J.* **1996**, *2*, 1221. (b) Shin, J. H.; Churchill, D. G.; Bridgewater, B. M.; Pang, K.; Parkin, G. *Inorg. Chim. Acta* **2006**, *359*, 2942. (c) Shin, J. H.; Savage, W.; Murphy, V. J.; Bonanno, J. B.; Churchill, D. G.; Parkin, G. *J. Chem. Soc., Dalton Trans.* **2001**, 1732. (d) Mathur, P.; Ahmed, M. O.; Dash, A. K.; Kaldis, J. H. *Organometallics* **2000**, *19*, 941. (e) Wardle, R. W. M.; Bhaduri, S.; Chau, C. N.; Ibers, J. A. *Inorg. Chem.* **1988**, *27*, 1747. (f) Eichhorn, B. W.; Gardner, D. R.; Nichols-Ziebarth, A.; Ahmed, K. J.; Bott, S. G. *Inorg. Chem.* **1993**, *32*, 5412. (g) Ansari, M. A.; Ibers, J. A. *Coord. Chem. Rev.* **1990**, *100*, 223. (h) Wardle, R. W. M.; Chau, C. N.; Ibers, J. A. *J. Am. Chem. Soc.* **1987**, *109*, 1859.

(23) (a) Rabinovich, D.; Parkin, G. *Inorg. Chem.* **1995**, *34*, 6341. (b) Christou, V.; Arnold, J. *Angew. Chem., Int. Ed. Engl.* **1993**, *32*, 1450. (c) Parkin, G. Terminal Chalcogenido Complexes of the Transition Metals. In *Prog. Inorg. Chem.*; Karlin, K. D., Ed.; John Wiley & Sons, Inc.: Hoboken, NJ, 1997; p 1. (d) Shin, J. H.; Parkin, G. *Organometallics* **1995**, *14*, 1104. (e) Rabinovich, D.; Parkin, G. *Inorg. Chem.* **1994**, *33*, 2313. (f) Johnson, A. R.; Davis, W. M.; Cummins, C. C.; Serron, S.; Nolan, S. P.; Musaev, D. G.; Morokuma, K. *J. Am. Chem. Soc.* **1998**, *120*, 2071.

(24) (a) Murphy, V. J.; Rabinovich, D.; Halkyard, S.; Parkin, G. *J. Chem. Soc., Chem. Commun.* **1995**, 1099. (b) Howard, W. A.; Waters, M.; Parkin, G. *J. Am. Chem. Soc.* **1993**, *115*, 4917. (c) Fischer, J. M.; Piers, W. E.; MacGillivray, L. R.; Zaworotko, M. J. *Inorg. Chem.* **1995**, *34*, 2499.

(25) Reed, A. E.; Curtiss, L. A.; Weinhold, F. *Chem. Rev.* **1988**, *88*, 899.

(26) (a) Bader, R. W. B. *Atoms in Molecules: A Quantum Theory*; Oxford University Press: Oxford, U.K., 1990. (b) Matta, C. F.; Boyd, R. J. *The Quantum Theory of Atoms in Molecules*; Wiley-VCH: Weinheim, Germany, 2007.

(27) Frenking, G.; Bickelhaupt, M. F. The EDA Perspective of Chemical Bonding. In *The Chemical Bond: Fundamental Aspects of Chemical Bonding*; Frenking, G., Shaik, S., Eds.; Wiley-VCH Verlag GmbH & Co. KGaA: Weinheim, 2014.

(28) $[U(O)(E)(NR_2)_3]^-$ complexes have formally 24-electrons shared by the actinide center in the Lewis structure notation, going thus beyond the "18-electron principle". See, e.g.: (a) Hrobárik, P.; Straka, M.; Pyykko, P. *Chem. Phys. Lett.* **2006**, *431*, 6. (b) Dognon, J. P.; Clavaguera, C.; Pyykko, P. *Angew. Chem., Int. Ed.* **2007**, *46*, 1427.

(29) Gopinathan, M. S.; Jug, K. *Theor Chim Acta* **1983**, *63*, 497.

(30) Herrmann, W. A.; Kneuper, H. J. *J. Organomet. Chem.* **1988**, *348*, 193.

(31) Awere, E. G.; Passmore, J.; White, P. S. *J. Chem. Soc., Dalton Trans.* **1993**, 299.

(32) Duddeck, H. *Prog. Nucl. Magn. Reson. Spectrosc.* **1995**, *27*, 1.

(33) Note that the term "paramagnetic shielding" is unrelated to the effect of unpaired electrons referred to as paramagnetic NMR spectroscopy.

(34) (a) Ramsey, N. F. *Phys. Rev.* **1950**, *78*, 699. (b) Karplus, M.; Pople, J. A. *J. Chem. Phys.* **1963**, *38*, 2803. (c) Atkins, P. W.; Friedman, R. S. *Molecular Quantum Mechanics*, 3rd ed.; Oxford University Press: Oxford, U.K., 1997.

(35) See also Supporting Information for a brief description of the Ramsey's equation and its simplified form.

(36) Autschbach, J. *J. Chem. Phys.* **2008**, *128*, 164112.

(37) Correlations of NMR chemical shifts with a QTAIM delocalization index were recently reported in (a) Vícha, J.; Foroutan-Nejad, C.; Pawlak, T.; Munzarová, M. L.; Straka, M.; Marek, R. *J. Chem. Theory Comput.* **2015**, *11*, 1509. (b) Greif, A. H.; Hrobárik, P.; Hrobáriková, V.; Arbuznikov, A. V.; Autschbach, J.; Kaupp, M. *Inorg. Chem.* **2015**, *54*, 7199.

(38) (a) Harris, R. K.; Becker, E. D.; Cabral De Menezes, S. M.; Goodfellow, R.; Granger, P. *Pure Appl. Chem.* **2001**, *73*, 1795. (b) Harris, R. K.; Becker, E. D.; Cabral De Menezes, S. M.; Granger, P.; Hoffman, R. E.; Zilm, K. W. *Pure Appl. Chem.* **2008**, *80*, 59.

(39) *SMART Apex II*, Version 2.1; Bruker AXS Inc.: Madison, WI, 2005.

(40) *SAINT Software User's Guide*, Version 7.34a; Bruker AXS Inc.: Madison, WI, 2005.

(41) Sheldrick, G. M. *SADABS*; University of Gottingen: Gottingen, Germany, 2005.

(42) *SHELXTL PC*, Version 6.12; Bruker AXS Inc.: Madison, WI, 2005.

(43) (a) Perdew, J. P.; Burke, K.; Ernzerhof, M. *Phys. Rev. Lett.* **1996**, *77*, 3865. (b) Perdew, J. P.; Burke, K.; Ernzerhof, M. *Phys. Rev. Lett.* **1997**, *78*, 1396. (c) Adamo, C.; Barone, V. *Chem. Phys. Lett.* **1998**, *298*, 113.

(44) Grimme, S.; Antony, J.; Ehrlich, S.; Krieg, H. *J. Chem. Phys.* **2010**, *132*, 1456.

(45) Grimme, S.; Ehrlich, S.; Goerigk, L. *J. Comput. Chem.* **2011**, *32*, 1456.

(46) *Turbomole*, version 6.3.1, University of Karlsruhe and Forschungszentrum Karlsruhe, GmbH, 1989–2007, TURBOMOLE GmBH since 2007; http://www.turbomole.com.

(47) (a) Cao, X. Y.; Dolg, M. *J. Mol. Struct.: THEOCHEM* **2004**, *673*, 203. (b) Andrae, D.; Haussermann, U.; Dolg, M.; Stoll, H.; Preuss, H. *Theor Chim Acta* **1990**, *77*, 123.

(48) Weigend, F.; Ahlrichs, R. *Phys. Chem. Chem. Phys.* **2005**, *7*, 3297.

(49) *Amsterdam Density Functional (ADF)*, version 2014.07; SCM, Theoretical Chemistry, Vrije Univeriteit: Amsterdam, Netherlands, 2015; http://www.scm.com.

(50) (a) Wolff, S. K.; Ziegler, T. *J. Chem. Phys.* **1998**, *109*, 895. (b) Wolff, S. K.; Ziegler, T.; van Lenthe, E.; Baerends, E. J. *J. Chem. Phys.* **1999**, *110*, 7689.

(51) Klamt, A.; Schuurmann, G. *J. Chem. Soc., Perkin Trans. 2* **1993**, 799.

(52) Glendening, E. D.; Badenhoop, J. K.; Reed, A. E.; Carpenter, J. E.; Bohmann, J. A.; Morales, C. M.; Landis, C. R.; Weinhold, F. *NBO 6.0*; Theoretical Chemistry Institute, University of Wisconsin: Madison, WI, 2013; http://nbo6.chem.wisc.edu/.

(53) Frisch, M. J. et al. *Gaussian 09*, revision D.01; Gaussian, Inc.: Wallingford, CT, 2009 (see the Supporting Information for full reference).

(54) (a) Lu, T. *Multiwfn: A Multifunctional Wave Function Analyzer*, version 3.3.7; 2015; http://multiwfn.codeplex.com;. (b) Lu, T.; Chen, F. W. *J. Comput. Chem.* **2012**, *33*, 580.

(55) te Velde, G.; Bickelhaupt, F. M.; Baerends, E. J.; Guerra, C. F.; Van Gisbergen, S. J. A.; Snijders, J. G.; Ziegler, T. *J. Comput. Chem.* **2001**, *22*, 931.

DOI: 10.1021/jacs.5b07767
J. Am. Chem. Soc. 2016, 138, 814–825